53

A SIMPLE DESCRIPTION OF TWO-DIMENSIONAL NMR SPECTROSCOPY*

Ad Bax

Laboratory of Chemical Physics
National Institute of Arthritis, Diabetes
and Digestive and Kidney Diseases
National Institutes of Health
Bethesda, Maryland 20205, USA

	Page
I. Introduction	167
A. Sampling Frequency and Sensitivity	168
B. Lineshapes and Transform Techniques	170
C. Two-dimensional Quadrature and Absorption Mode	172
D. Coherence Transfer by Means of Radiofrequency Pulses	173
II. Homonuclear Shift Correlation through Scalar Coupling	175
III. Homonuclear Chemical Shift Correlation through Cross Relaxation	177
IV. Indirect Detection of ^{15}N through Multiple Quantum Coherence	178
V. Discussion	182
References	182

I. INTRODUCTION

The concept of two-dimensional (2D) Fourier transformation in NMR was first introduced by Jeener (1) in 1971. Since that time, several hundred different 2D pulse schemes have been proposed in the literature. The selection of experiments that will be described is based on the insight they provide into the basis and generality of 2D NMR, and also on the importance for solving the most common types of problems.

The experiments that will be described here are (a) 2D homonuclear shift correlation through scalar coupling (COSY), (b) 2D cross relaxation spectroscopy based on the nuclear Overhauser effect (NOESY) and (c) heteronuclear chemical shift correlation of ^{1}H and ^{15}N chemical shifts through multiple quantum coherence.

Before addressing those experiments, an introduction into the principles and general aspects of two-dimensional NMR will be presented. The original 2D experiment, proposed by Jeener (1), will be discussed for the simple case of non-coupled nuclear spins, for example, the protons in chloroform. This will illustrate how a 2D Fourier transformation is accomplished and also which type of data presentation (absorptive / dispersive / absolute value) is generally preferrable. Jeener's original sequence is depicted in Figure 1. At the end of the preparation period, which is sufficiently long to establish a (close to) thermal equilibrium situation, a 90° pulse applied along the -y axis of the rotating frame ($90°_{-y}$ pulse) rotates the magnetization to a position parallel to the x axis (Figure 2a). The system then evolves (usually in an unperturbed fashion) for a time t_1, which is generally referred to as the evolution period. During this period the magnetization rotates through an angle $\Omega_1 t_1$, where Ω_1 is the angular rotation frequency of the magnetization considered (Figure 2b). At the end

---

*Part of this manuscript has been published in the proceedings of the *NATO Advanced Study Institute on NMR in Living Systems*, Sicily, Italy, 1984.

values are separated by an amount Δt_1, this will give a spectral width equal to $1/(2\Delta t_1)$ after Fourier transformation with respect to t_1.

In a regular one-dimensional Fourier transform experiment, the signal-to-noise ratio for a single time-domain data point can be very poor;

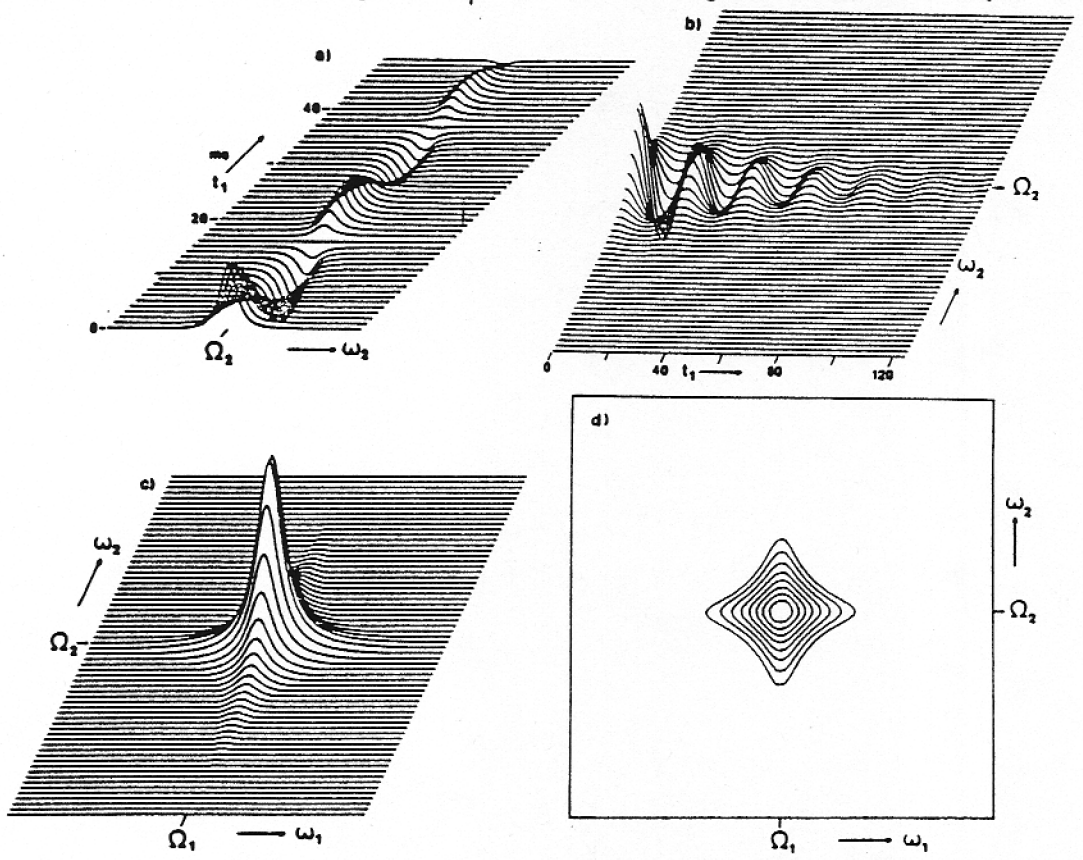

Figure 3. (a) A set of spectra obtained with the sequence of Figure 1b for increasing durations of the evolution period, t_1. (b) Transposed data matrix of Figure 3a. (c) Fourier transform of the interferograms of Figure 3b resulting in a two-dimensional stacked line spectrum. (d) The spectrum of Figure 3c, represented as a contour plot.

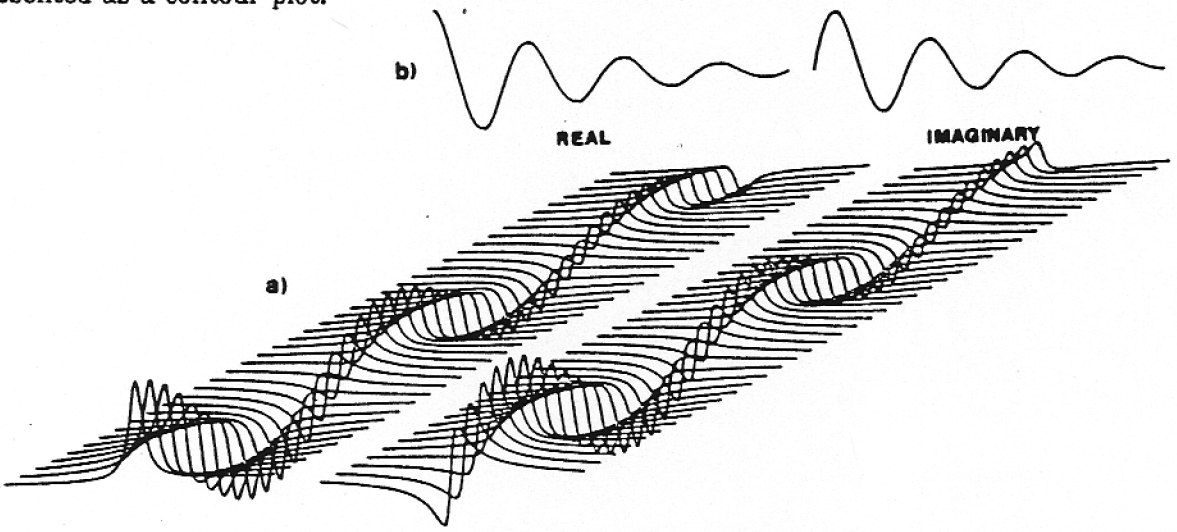

Figure 4. (a) A set of phase-modulated spectra. The phase of the resonance is a linear function of the duration of the evolution period, t_1. Both the real and imaginary halves of the spectra are shown. (b) Complex interferogram taken at $\omega_2 = \Omega_2$. The first half of the interferogram represents a t_1 section through the real halves of the spectra in Figure 4a, and the second half is the interferogram through the imaginary halves. A quadrature Fourier transform of this complex interferogram determines the sign and the magnitude of the modulation frequency.

however, the Fourier transformation takes the signal energy of all data points and puts it all into one (or several) narrow resonance line(s). Similarly, if for each t_1 value in a 2D experiment a spectrum with poor signal-to-noise ratio is obtained, the second Fourier transformation with respect to t_1 combines the signal energy of a particular resonance from all spectra obtained for different t_1 values, and concentrates it into one narrow line in the 2D spectrum. Therefore, the sensitivity of 2D NMR is not necessarily lower than for the one-dimensional experiment.

In certain types of experiments one tries to transfer magnetization from one resonance to another by means of a coherent process or by means of cross relaxation or chemical exchange (to be discussed later). In this case the sensitivity of 2D NMR can become rather poor if the transfer process is not very efficient (as is the case in coherent transfer through non-resolved couplings or in the case of slow cross relaxation or chemical exchange). However, the analogous one-dimensional experiment also suffers in sensitivity in this case.

If sensitivity is a crucial problem, the two rules that should always be obeyed are:

1. The acquisition time in the t_2 dimension, $t_{2\,max}$, should be at least equal to 1.5 T_2.
2. The acquisition time in the t_1 dimension, $t_{1\,max}$, should be chosen as short as possible, i.e. not longer than absolutely necessary to obtain enough resolution in the ω_1 dimension after Fourier transformation. Since the signal decays as a function of the time t_1, spectra taken for short t_1 values contribute more to the 2D resonance intensity (and sensitivity) than spectra obtained for t_1 values on the order of $T_2^{(1)}$ or longer.

More discussions on sensitivity of 2D NMR can be found in the literature (3-6).

B. Lineshapes and Transform Techniques

The spectrum in Figure 3c represents the cosine Fourier transform with respect to t_1 of the real part of eqn. 2. If interferograms through the real and imaginary halves of the $S(t_1,\omega_2)$ are Fourier transformed separately, this gives:

$$S(\omega_1,\omega_2) = A_1(\omega_1)A_2(\omega_2) + iA_1(\omega_1)D_2(\omega_2) + jD_1(\omega_1)A_2(\omega_2) + jiD_1(\omega_1)D_2(\omega_2) \qquad (4)$$

where "j" has the same meaning as "i", but refers to the imaginary data in the F_1 dimension. $A_1(\omega_1)$ and $D_1(\omega_1)$ are defined analogous to eqn. 3. The four terms at the right hand side of eqn. 4 are also known as S^{cc}, S^{cs}, S^{sc} and S^{ss} in the older literature (2,7). Clearly, only one of the four parts (S^{cc}), shows the desirable 2D absorption mode lineshape.

The signal of eqn. 2 is modulated in amplitude by a cosine function. It is impossible to tell from the second Fourier transformation whether the modulation frequency, Ω_1, is positive or negative. Of course, for this simple case one knows that $\Omega_1 = \Omega_2$, and if quadrature detection during t_2 is employed, the sign of the modulation frequency is determined. However, in many experiments this is not the case and in order to avoid confusion, one has to make sure that all modulation frequencies have the same sign by positioning the transmitter frequency at either the low or high field side of the spectrum. Because of sensitivity considerations, quadrature detection in the t_2 dimension is always necessary, and data storage space is wasted if the transmitter frequency is not set at the center of the spectrum. Also, radiofrequency offset effects may become prohibitively severe in certain types of experiments.

A simple way around this problem is the introduction of artificial phase modulation, to be described below. If a second experiment, "$90^\circ_{-y} - t_1 - 90^\circ_{y}$ – acquire(t_2)" is performed, the signal detected in this second experiment will start out along the y axis (at $t_2 = 0$) and is modulated in amplitude by $\sin(\Omega_1 t_1)$:

$$\begin{aligned} s'(t_1,t_2) &= M_0\sin(\Omega_1 t_1)\exp[i(\Omega_2 t_2 + \pi/2)] \times \\ &\quad \exp(-t_1/T_2^{(1)})\exp(-t_2/T_2^{(2)}) \\ &= iM_0\sin(\Omega_1 t_1)\exp(i\Omega_2 t_2) \times \\ &\quad \exp(-t_1/T_2^{(1)})\exp(-t_2/T_2^{(2)}) \end{aligned} \qquad (5)$$

Adding the results of the two experiments, eqns. 5 and 1, directly together and omitting the relaxation terms gives:

$$s^+(t_1,t_2) = M_0\exp(i\Omega_1 t_1)\exp(i\Omega_2 t_2) \qquad (6)$$

Eqn. 6 represents a signal of which the phase at time $t_2 = 0$ is a linear function of the duration of evolution period, t_1. Fourier transformation with respect to t_2 will yield a resonance at $\omega_2 = \Omega_2$, and with phase $\Omega_1 t_1$:

$$S^+(t_1,\omega_2) = M_0[\cos(\Omega_1 t_1)A_2(\omega_2) - \sin(\Omega_1 t_1)D_2(\omega_2)] +$$

$$iM_0[\cos(\Omega_1 t_1)D_2(\omega_2)+\sin(\Omega_1 t_1)A_2(\omega_2)] \qquad (7)$$

A set of spectra obtained this way for a series of t_1 values, is sketched in Figure 4. Both the real and imaginary halves of those spectra are shown. An interferogram taken at $\omega_2 = \Omega_2$ does not contain any of the dispersive components since $D_2(\Omega_2)=0$, and this interferogram is described by:

$$S^*(t_1,\Omega_2) = M_0[\cos(\Omega_1 t_1)+i\sin(\Omega_1 t_1)]T_2^{(2)} \qquad (8)$$

where the real part represents the interferogram taken through the real part of eqn. 6, and the imaginary part of eqn. 8 is the interferogram taken through the imaginary parts of the $s^*(t_1,\Omega_2)$ spectra. This complex interferogram is sketched in Figure 4b. A complex Fourier transformation of eqn. 8 can be made, and the sign of the modulation freguency, Ω_1, is automatically determined. Any interferogram taken at an ω_2 value different from Ω_2, will have non-zero contributions from $D_2(\omega_2)$, and Fourier transformation with respect to t_1 of this $D_2(\omega_2)$ contribution will yield a resonance in the F_1 dimension that is 90° out of phase relative to the interferogram taken at $\omega_2 = \Omega_2$. The full 2D Fourier transform of eqn. 6 is given by:

$$S^*(\omega_1,\omega_2) =$$

$$M_0[A_1(\omega_1)A_2(\omega_2)-D_1(\omega_1)D_2(\omega_2)] \; + \; iM_0[A_1(\omega_1)D_2(\omega_2)+D_1(\omega_1)A_2(\omega_2)] \qquad (9)$$

Clearly, both the real and imaginary part of this function are mixtures of absorption and dispersion. The real part of eqn. 9 is sketched in Figure 5. The resonance shows a so-called "phase twist" lineshape (2), and cannot be phased to the pure absorption mode. In practice, an absolute value mode calculation is usually made before display:

$$\text{Absolute value} = [Re^2+Im^2]^{\frac{1}{2}} \qquad (10)$$

Since the tails of an absolute value mode resonance decrease proportional to $1/|\omega-\Omega|$, this resonance shows undesirable tails, decreasing resolution.

Nevertheless, this artificially induced phase modulation is currently the most common way of operation for most 2D experiments. The software of most commercial spectrometers assume data in a 2D experiment to be phase-modulated, and the data matrix transposition routine automatically places the imaginary half of the interferogram behind the real half (as depicted in Figure 4b), ready for a second complex Fourier transformation, this time with respect to t_1.

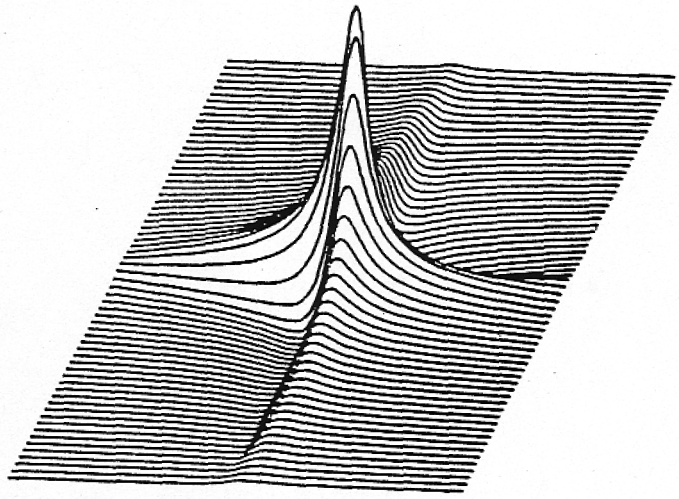

Figure 5. phase-twisted line shape obtained by Fourier transformation with respect to t_1 of the matrix of Figure 4a.

The strong tailing of the absolute value mode lineshape can be suppressed by the use of appropriate digital filtering. All those filters have in common that they reshape the envelope amplitude of the time domain data to decay in a near symmetrical fashion from the midpoint of the FID (8). Filters commonly used for this purpose are the sine bell function (9), the "pseudo-echo window" (10) and the convolution difference filter (11). Figure 6 compares the contour plots for a regular absolute value mode line-shape, and one that has been obtained after the time domain data were multiplied by a sine bell in both dimensions. Unfortunately, the sensitivity generally suffers severely from the use of such resolution enhancement filtering functions (the COSY experiment, to be discussed later, can under certain conditions be an exception to this rule).

Although phase modulated experiments are experimentally very convenient, sensitivity and resolution suffer. Another disadvantage of artificial phase modulation, not discussed above nor mentioned explicitly in the literature, is that only half of the available signal is used: if the

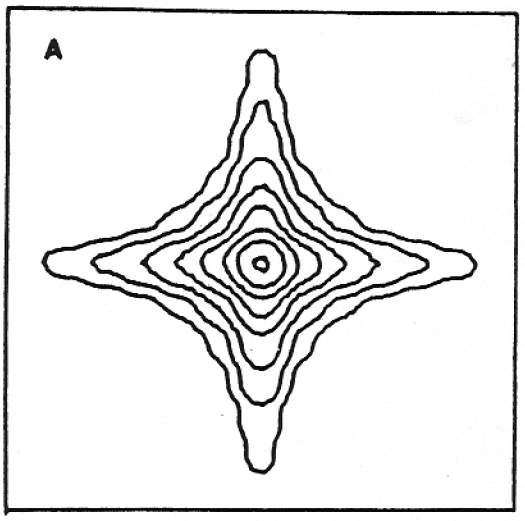

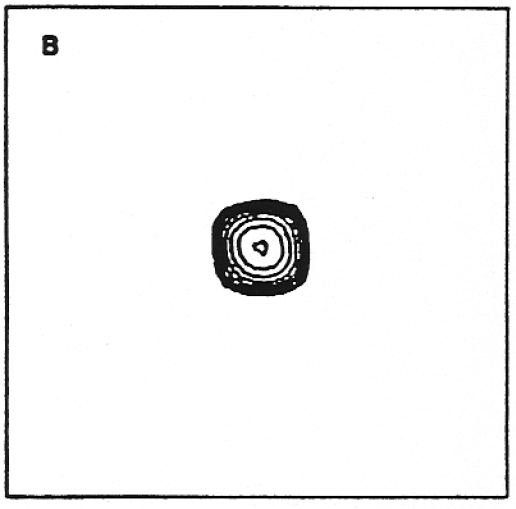

Figure 6. Comparison of the contour plots of absolute value mode line shapes. (a) Line shape obtained after an absolute value mode calculation of a signal that has been multiplied by a negative exponential with a time constant $T_2 = AT/3$, where AT is the duration of the acquisition time. (b) Line shape obtained if the time domain signal is multiplied by a sine bell function. The lowest contour level is taken at 1/12th of the peak height.

difference of the two experiments (eqn. 1 and eqn. 5) were taken, this gives a signal of the shape:

$$s^-(t_1,t_2) = M_0\exp(-i\Omega_1 t_1)\exp(i\Omega_2 t_2) \quad (11)$$

The noise in eqns. 6 and 11 is in principle independent. If only the sum or the difference is taken, half of the available signal is wasted!

C. Two-dimensional Quadrature and Absorption Mode

As explained above, absorption mode 2D spectra can only be recorded if the transmitter is placed at either the low or high field side of the spectrum. Since data acquisition during t_2 has to be done in quadrature (for sensitivity reasons), this type of experiment is very inefficient as far as data storage is concerned. Also, pulse imperfections due to resonance offset can become severe. A more efficient way to obtain a 2D absorption mode spectrum in 2D quadrature, was first introduced by Muller and Ernst (12) and by Freeman et al.(13) and also by States et al.(14). This so-called hypercomplex Fourier transformation approach will be described below.

Consider again the pulse sequence of Figure 1 and the signal of eqn. 1. A second experiment, $90^\circ_{-x} - t_1 - 90^\circ_{x} - \text{acquire}(t_2)$, is performed. The signal in the second experiment is initially ($t_2 = 0$) also along the x axis, but is modulated in amplitude by $\sin(\Omega_1 t_1)$. The FID's obtained in the two experiments, $s(t_1,t_2)$ and $s'(t_1,t_2)$, are *not* co-added this time, but stored in separate locations in memory. Hence, for every t_1 value, two spectra are recorded, one modulated by a cosine and the other one by a sine function. Fourier transformation of the two sets of spectra gives:

$$S(t_1,\omega_2) = M_0\cos(\Omega_1 t_1)[A_2(\omega_2) + iD_2(\omega_2)] \quad (12a)$$

$$S'(t_1,\omega_2) = M_0\sin(\Omega_1 t_1)[A_2(\omega_2) + iD_2(\omega_2)] \quad (12b)$$

The simple but crucial trick is to replace the imaginary part of $S(t_1,\omega_2)$ by the real part of $S'(t_1,\omega_2)$, yielding:

$$S^t(t_1,\omega_2) = M_0\exp(i\Omega_1 t_1)A_2(\omega_2) \quad (13)$$

A set of those spectra is shown in Figure 7. Complex Fourier transformation with respect to t_1 of eqn. 13 gives for the real part:

$$S^t(t_1,\omega_2) = M_0A_1(\omega_1)A_2(\omega_2) \quad (14)$$

which represents a 2D absorption mode resonance. Undoubtedly this will become the accepted way of data processing for most 2D NMR

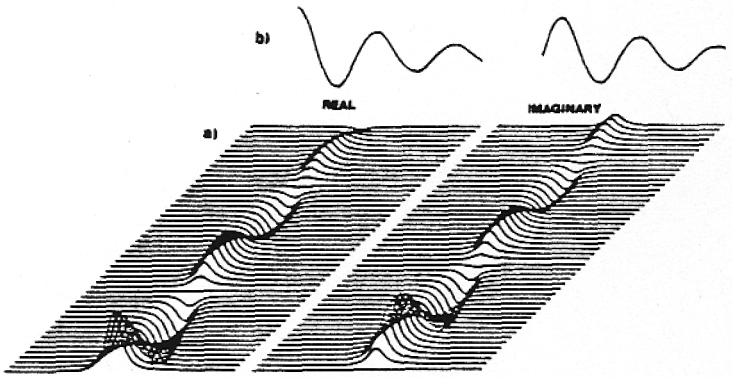

Figure 7. (a) The left halves of the spectra are the absorption parts of the spectra obtained with an experiment where the resonance is modulated in amplitude by a cosine function. The dispersive parts of these spectra have been replaced by the absorptive part of the spectra obtained with a second experiment, where the resonances are modulated in amplitude by a sinusoidal function. (b) Complex interferogram taken at $\omega_2 = \Omega_2$.

experiments in the near future.

A slightly different approach for the same problem of two-dimensional quadrature and absorption mode has recently been proposed by Bodenhausen et al. (15) and is based on an idea first introduced by the Pines group (16). In this so-called TPPI method (Time Proportional Phase Increment), the rf phases of all preparation pulses are incremented by 90° for consecutive t_1 values. This causes the apparent modulation frequency to be increased (or decreased) by $(2\Delta t_1)^{-1}$, and makes it appear that all modulation frequencies are positive (or negative), and therefore allows a real (cosine) Fourier transformation with respect to t_1. Although, at first sight, the hypercomplex and the TPPI methods seem totally different, a closer analysis shows that the methods are almost identical. Also from a practical point of view there is little difference: identical size data matrices are required and identical data acquisition times are needed for the two methods, giving indistinguishable resolution and sensitivity in the final spectrum. Comparing the two methods is similar to comparing the different ways in which most commercial spectrometers versus most of the Bruker spectrometers acquire quadrature information in a one-dimensional spectrum. In most spectrometers two data points, containing the x and y information, are sampled simultaneously, whereas in most Bruker spectrometers quadrature information is obtained by sampling at twice the rate, and incrementing the receiver reference phase by 90° for consecutive sampling points, taking only one data point at a time (17).

Lines in an absorption mode spectrum can be so narrow that digitization of the resonances becomes a problem. In this case, the highest point of a resonance in a 2D spectrum can be reduced by as much as 70%, apparently decreasing the intensity of a resonance in a contour plot dramatically. This effect has been observed experimentally. A simple solution to this problem is to zero fill by a number of data points equal to the number of signal-containing data points, prior to Fourier transformation. In absolute value mode spectra, lines are broadened sufficiently by the absolute value mode calculation and use of this zero-filling procedure is therefore usually not essential.

D. Coherence Transfer by Means of Radiofrequency Pulses

Classical vector pictures have been used for over three decades to explain the mechanisms on which many NMR experiments rely (18). However, for a description of most of the newer type pulse sequences, applied to coupled spin systems, straightforward application of those vector pictures leads to erroneous results. Ernst and coworkers (19) and other workers (20,21) have introduced a formalism that does allow the use of vector pictures to analyze the behavior of a coupled spin system. This operator formalism based vector picture is more complicated than is the use of the classical picture based on the Bloch equations, but is much less tedious than use of the density matrix formalism. The new approach will be briefly discussed for a homonuclear weakly coupled two-spin system. Two weakly coupled spins, A and B, will be considered.

The total net magnetization of spin A equals the vector sum of the magnetizations of the two

doublet components (Figure 8). As in the classical vector picture, the vector sum of the two

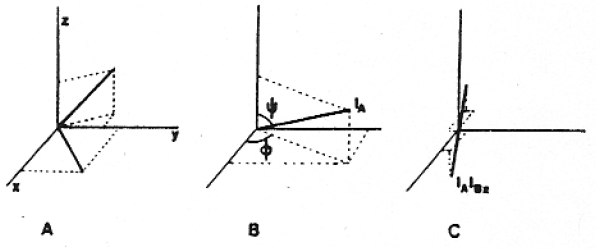

Figure 8. (a) Arbitrary orientation of the two magnetization vectors of the doublet components of nuclei, A. (b) The vector sum of the two doublet components. (c) The difference between the two doublet components, representing antiphase magnetization.

doublet components is represented by a vector I_A that can be decomposed in the standard fashion into its components along the principal axes of the rotating frame (Figure 8b):

$$I_A = \cos(\Psi)I_{Az} + \sin(\Psi)\cos(\phi)I_{Ax} + \sin(\Psi)\sin(\phi)I_{Ay} \quad (15)$$

This vector sum is the sum of the in-phase components of the two doublet magnetization vectors. The antiphase components of the two doublet magnetization vectors do not contribute to I_A in this picture. Since those components are opposite to each other, they do not contribute to macroscopic observable magnetization. Of the antiphase components of spin A, one component corresponds to spin B in the m=1/2 spin state, and the other to the m=-1/2 state. This antiphase magnetization can then formally be written as $2I_AI_{Bz}$. The factor "2" in this product is needed for normalization. The new formalism treats the individual terms in such a product as normal magnetization, in the classical way.

In order to make the description more explicit: consider the effect of a 90°_x pulse applied to the two-spin system that is initially in thermal equilibrium. The magnetization (I_{Az} + I_{Bz}) gets rotated to a position parallel to the -y axis*, and thus creates $-(I_{Ay}+I_{By})$. The magnetization of the two nuclei can be considered separately, and we will concentrate on the fate of the A spin magnetization. This will rotate with angular frequency, Ω_A, about the z axis and the two doublet components will periodically (with period 1/J) get in antiphase. These two processes can be considered separately:

$$I_{Ay} \xrightarrow{\Omega_A I_{Az} t} I_{Ay}\cos(\Omega_A t) - I_{Ax}\sin(\Omega_A t) \quad (16a)$$

$$I_{Ay} \xrightarrow{2\pi J I_{Az} I_{Bz} t} I_{Ay}\cos(\pi J t) - 2I_{Ax}I_{Bz}\sin(\pi J t) \quad (16b)$$

$$I_{Ax} \xrightarrow{2\pi J I_{Az} I_{Bz} t} I_{Ax}\cos(\pi J t) + 2I_{Ay}I_{Bz}\sin(\pi J t) \quad (16c)$$

Substitution of eqns. 16b and 16c in 16a then gives the complete evolution of the magnetization. The interesting terms in eqn. 16 are the products $I_{Ax}I_{Bz}$,and $I_{Ay}I_{Bz}$. Consider a 90° pulse applied to such a term:

$$I_{Ax}I_{Bz} \xrightarrow{90^\circ_y} -I_{Az}I_{Bx} \quad (17a)$$

$$I_{Ax}I_{Bz} \xrightarrow{90^\circ_x} -I_{Ax}I_{By} \quad (17b)$$

eqn. 17a shows how antiphase A spin magnetization gets converted into antiphase B spin magnetization by a 90° pulse applied perpendicular to the doublet magnetization vectors. This important result is the basis of Jeener's original experiment when applied to a homonuclear coupled spin system. Eqn. 17b contains the product $I_{Ax}I_{By}$ and is harder to visualize; this term represents so-called two-spin coherence, a combination of zero- and double quantum coherence. The time evolution of the product equals the product of the time evolution of the individual terms; i.e. the time evolution of $I_{Ax}I_{By}$ is given by

$$I_{Ax}I_{By} \xrightarrow{\Omega_A t I_{Az} + \Omega_B t I_{Bz}} [\cos(\Omega_A t)I_{Ax} + \sin(\Omega_A t)I_{Ay}] \times [\cos(\Omega_B t)I_{By} - \sin(\Omega_B t)I_{Bx}] \quad (18)$$

The operator formalism is easily extended to more spins by considering product terms of all spins involved. For a more complete description of this extremely useful formalism, the reader is

---

*In order to be consistent with conventions used in the paper by Sorensen et al.(19), describing the operator formalism, we adopt here the convention that a 90°_x rotates the magnetization anti-clockwise around the x axis, i.e. from the z to the -y axis.

referred to the literature (19-21).

II. HOMONUCLEAR SHIFT CORRELATION THROUGH SCALAR COUPLING

Jeener's original 2D pulse scheme can be considered as a convenient alternative for the conventional one-dimensional double resonance experiments, and is often referred to as the COSY (COrrelated SpectroscopY) experiment. A complete quantum mechanical description of the experiment was presented by Aue et al.(22) but did not contribute much to the popularity of the experiment. Only in the early 1980's the widespread applicability of this technique was realized (23-27). The basic pulse scheme has already been discussed in the previous sections. Here a $90^\circ_x - t_1 - 90^\circ_\phi -$ acquire(t_2) pulse scheme is used, where the phase ϕ of the final pulse and the mode of data acquisition are selected as indicated in Table 1. This means that a minimum of four experiments is performed for each t_1 value with the phase of the final 90° pulse incremented by 90° each time and data alternately added to and subtracted from memory. This way of phase cycling results in detection of the $s^-(t_1,t_2)$ signal of eqn. 11, often referred to as the coherence transfer echo (28). The occurrence of the echo is easily understood by considering that in eqn. 11, Ω_1 and Ω_2 have approximately the same value (in the laboratory frame). Therefore, at time $t_1 = t_2$, the phase of the magnetization, $\exp[i(\Omega_2 t_2 - \Omega_1 t_1)]$, is to first order independent of the magnetic field strength, i.e. independent of magnetic field inhomogeneity, and consequently an echo will occur. The entire four-step experiment is often repeated four times with the phases of all radiofrequency pulses and receiver incremented by 90° each time. This additional so-called CYCLOPS cycling (29) eliminates imperfections in the quadrature detection system of the spectrometer which otherwise may cause small mirror image signals about the $\omega_2 = 0$ and $\omega_1 = 0$ axes.

Table 1. Cycling of the phase of the observe pulse, ϕ, and of the receiver in the various steps of the COSY experiment in order to obtain phase modulation and to detect the coherence transfer echo.

Step	ϕ	Receiver
1	x	+
2	y	-
3	-x	+
4	-y	-

The COSY experiment relies on transfer of magnetization from spin A to spin X by the second 90° pulse in Jeener's experiment, and can only occur if spin A and X are mutually coupled. The mechanism for this magnetization transfer has been discussed in the previous section: eqn. 17a shows how spin A doublet components that are in antiphase with respect to spin X are transferred into X spin doublet components that are in antiphase with respect to spin A. The amount of antiphase A-spin magnetization present before the second 90° transfer pulse depends on $\sin(\pi J_{AX} t_1)$. The magnetization observed during t_2 starts out in antiphase and is proportional to $\sin(\pi J_{AX} t_2)$. The time domain signal for the magnetization transferred from A to X is given by

$$s^-_{AX}(t_1,t_2) = M_0 \sin(\pi J_{AX} t_1) \sin(\pi J_{AX} t_2) \times \exp(-i\Omega_A t_1) \exp(i\Omega_X t_2) \quad (19)$$

Note that for very short t_1 values only very little magnetization is transferred from A to X. Rewriting:

$$\sin(\pi J t) = -i[\exp(i\pi J t) - \exp(-i\pi J t)]/2 \quad (20)$$

and substitution in eqn. 19 shows that the Fourier transformed signal $S^-(\omega_1,\omega_2)$ will show four peaks at $(\omega_1,\omega_2) = (\Omega_A \pm \pi J_{AX}, \Omega_X \pm \pi J_{AX})$, and that those resonances show antiphase relationships, as schematically indicated in Figure 9. Also indicated in Figure 9 are the "diagonal resonances," due to magnetization that is not transferred from A to X or from X to A, and which are 90° out of phase relative to the cross peaks. It is therefore impossible to phase all resonances in this spectrum simultaneously to the 2D absorption mode (unless the pulse scheme is altered (30)), and an absolute value mode calculation before display is therefore commonly used. The artificial phase modulation scheme

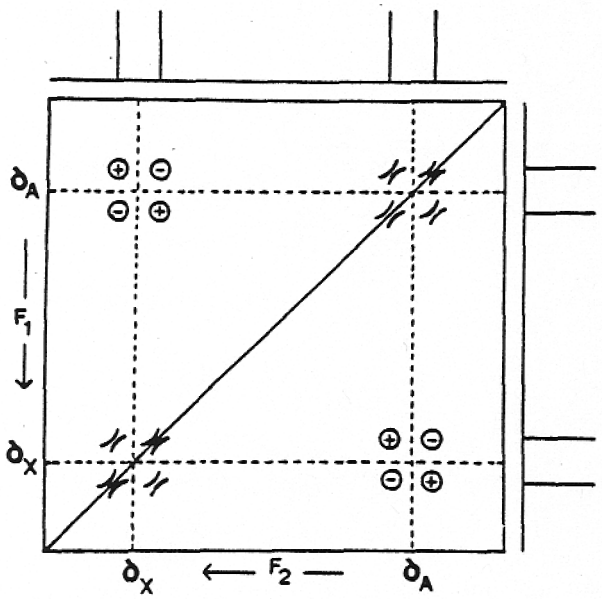

Figure 9. Schematic diagram of the 2D COSY spectra of an AX spin system. The four components of the AX cross multiplet are pairwise in antiphase, whereas the four diagonal multiplet components are 90° out of phase in both dimensions relative to the cross peaks.

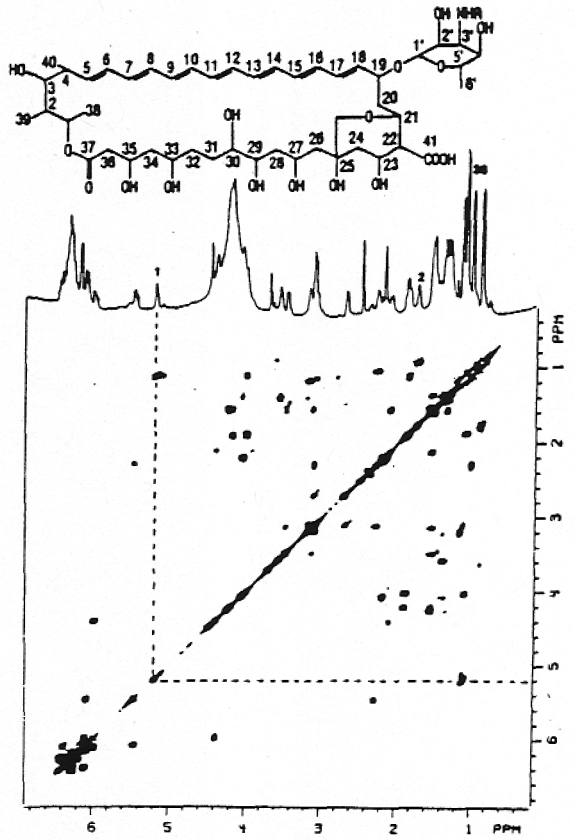

Figure 10. 500 MHz absolute value mode COSY spectrum of a sample of amphotericin B in DMSO-d_6. 16 experiments were performed for each t_1 value, and the total duration of the experiment was 4 h. A sine bell has been used in both dimensions prior to Fourier transformation.

(discussed before) therefore does not degrade performance of the experiment very much. Also, since the cross peak time domain signal has an envelope amplitude proportional to $\sin(\pi J_{AX} t_1)\sin(\pi J_{AX} t_2)$, and acquisition times in the t_1 and t_2 dimension are typically 100-300 ms, use of a sine bell digital filter is close to a matched filter for those signals and favors the sensitivity of the cross multiplets, meanwhile cutting down the intensity of redundant diagonal peaks which have a $\cos(\pi J_{AX} t_1)\cos(\pi J_{AX} t_2)$ dependence.

Figure 10 shows the COSY spectrum for a 25 mM solution of amphotericin B in DMSO-d_6, recorded on a Nicolet 500 MHz spectrometer. 512 t_1 increments of 300 μsec each were used, and 512 complex data points were acquired for each t_1 value. The artificial phase modulation scheme (Table 1) was employed and the total measuring time was 4 h. Note that in the regular one-dimensional spectrum many of the couplings are not or poorly resolved. However, a wealth of cross peaks can be observed in the 2D spectrum. For example, it is seen that proton 1 is coupled to methyl group 38 (broken line in Figure 10).

Many users of the COSY experiment are often puzzled by the absence or low intensity of certain cross peaks. For example, the cross peaks between protons 1 and 2 in Figure 10 have too low an intensity to be observed in the contour plot. In general, it is hard to calculate exactly how intense a cross multiplet will be, but two factors that are of major importance will be mentioned below.

1. A proton that is coupled to a large number of other protons will show rather low

intensity for its individual 1D multiplet components. In the COSY experiment, this low intensity will now be redistributed among all protons to which it is coupled by the mixing pulse, yielding very low intensity for the cross multiplets. The effect is particularly severe for cross peaks between two multiplets that both have a complicated multiplet structure.

2. If transverse relaxation times, T_2, are short compared with J_{AX}^{-1}, the transferred magnetization in eqn. 19 will never assume a large value and therefore only (vanishingly) low intensity cross peaks can be observed.

From point 1, it is clear that a large coupling does not necessarily give rise to an intense cross peak. However, if acquisition times $t_{1\,max}$ and $t_{2\,max}$ are chosen short (<100 ms) this will relatively emphasize cross peaks due to large scalar couplings. Recently, it has been shown that if the size of certain couplings can be estimated, a "designer" filter can be used to pick up those missing cross peaks (31).

III. HOMONUCLEAR CHEMICAL SHIFT CORRELATION THROUGH CROSS RELAXATION

In the COSY experiment, magnetization is transferred from one proton to another through the scalar coupling mechanism. This experiment relies on the existence of (partially) resolved scalar couplings. Another way to transfer magnetization between nuclei is the cross relaxation mechanism, which relies on the internuclear dipolar interaction. This mechanism is generally referred to as the nuclear Overhauser effect (NOE). The 2D pulse scheme that is based on the NOE effect is generally known as the NOESY experiment. This experiment was first proposed by Ernst, Jeener et al.(32,33). It is mentioned here that the same experiment can also be used for the investigation of chemical exchange processes. Obviously, no resolved couplings are needed for this experiment; the experiment tends to work very well for macromolecules which have a slow tumbling rate and therefore less ideal averaging of the dipolar coupling mechanism. This is the reason for strong cross relaxation and causes line broadening in the conventional 1D spectrum and also in the 2D spectrum.

The pulse scheme is sketched in Figure 11 and the mechanism on which this 2D experiment relies will be briefly discussed below. Assume for reasons of simplicity that all pulses in the scheme are applied along the x axis of the rotating frame, and consider a molecule with two spins A and B that have no mutual scalar coupling. The longitudinal magnetization of spin A, just after the second 90° pulse, is given by:

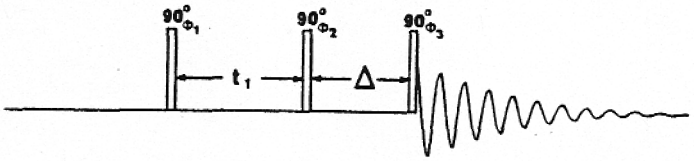

Figure 11. Pulse scheme of the 2D experiment to detect homonuclear cross relaxation and chemical exchange. The phases of the rf pulses , ϕ_1 and ϕ_2, and of the receiver are cycled according to Table 2, and the results of the odd and even steps are stored in separate locations in memory and processed as described in the text in order to obtain an absorption mode spectrum.

$$M_{zA}(t_1) = -M_{0A}\cos(\Omega_A t_1) \qquad (21)$$

During the mixing period of duration, Δ, cross relaxation with spin B takes place, changing the longitudinal B spin magnetization by an amount $C[M_{zA}(t_1) - M_{zB}(t_1)]$ and the A spin magnetization by the opposite amount, where C is a constant depending on the cross relaxation rate, the longitudinal relaxation rates, and the duration, Δ. Just before the final pulse, the longitudinal B spin magnetization is thus given by

$$M_{zB}(t_1) = f[M_{zB}(t_1)] + CM_{zA}(t_1) \qquad (22)$$

where $f[M_{zB}(t_1)]$ is a function depending on the relaxation of proton B during the delay, Δ, and on the modulation of the B spin magnetization by the first two pulses in the sequence. It is the second term at the right hand side of eqn. 22 that is the term of interest, since this term is due to cross relaxation from nucleus A to B. The final 90° pulse converts this term into transverse B magnetization which follows from eqns. 21 and 22:

$$s_{AB}(t_1, t_2) = CM_{0A}\cos(\Omega_A t_1)\exp(i\Omega_B t_2) \qquad (23)$$

Table 2. Phases ϕ_1 and ϕ_3 of the pulses in Fig. 11 in the various steps of the experiment. Phase ϕ_2 is x for all 16 steps. Data of odd and even steps are stored separately in the computer memory.

Step	ϕ_1	ϕ_3	Receiver
1	x	x	x
2	y	x	x
3	-x	x	-x
4	-y	x	-x
5	x	y	y
6	y	y	y
7	-x	y	-y
8	-y	y	-y
9	x	-x	-x
10	y	-x	-x
11	-x	-x	x
12	-y	-x	x
13	x	-y	-y
14	y	-y	-y
15	-x	-y	y
16	-y	-y	y

This signal is of the same shape as eqn. 1, and 2D Fourier transformation will therefore give a resonance at $(\omega_1,\omega_2)=(\Omega_A,\Omega_B)$. In contrast with the COSY experiment, diagonal and cross peaks in the 2D spectrum will all have the same phase, or exactly opposite phase, depending on the motional correlation time, τ_c. It is therefore strongly desirable to record the spectrum in the absorption mode, using the procedure outlined in Section IC. In order to eliminate transfer through scalar coupling (the COSY mechanism) further phase cycling is necessary. In practice a 16-step sequence (Table 2) is often used and additionally, this 16-step sequence is repeated four times in the CYCLOPS mode (29) in order to eliminate quadrature artifacts. Remaining coherent transfer through zero and triple quantum coherence, that is not cycled out this way can largely be eliminated by random fluctuation of Δ by a small amount (5%), provided that the frequency of this zero or triple quantum coherence is larger than $20/\Delta$ Hz.

If the cross relaxation is slow compared to the longitudinal relaxation, maximum transfer from spin A to B, and vice versa, occurs for a mixing time on the order of the shortest T_1 of the two spins involved. Hence, from a sensitivity point of view, a mixing time on the order of T_1 is optimum for the detection of cross peaks. However, if one wants to obtain quantitative information about the relaxation rates, one has to consider that the cross peak buildup rate (as a function of Δ) is non-linear (32-36). The simplest way around this problem is to consider only short mixing times, for which the NOE buildup is still in the linear region (35,36), but this approach necessarily leads to smaller cross peaks, i.e. lower sensitivity.

As an example, Figure 12 shows a contour plot of the 2D NOE spectrum of amphotericin B, showing a large number of cross peaks, obtained for a mixing time of 200 ms. Analysis of the cross peak network does not only provide assignment for all ^1H resonances in this compound, additional to that obtained from the COSY spectrum of Figure 10, but also gives information regarding the three-dimensional structure in solution.

IV. INDIRECT DETECTION OF ^{15}N THROUGH MULTIPLE QUANTUM COHERENCE

Detection of ^{15}N shifts is limited by its low NMR sensitivity, which is due to the small and negative value of the magnetogyric ratio and to the low natural abundance (0.37%). The fact that the magnetogyric ratio, γ, is negative can cause signal cancellation in the case of incomplete nuclear Overhauser enhancement. NMR sensitivity is approximately proportional to $\gamma^{5/2}$ (37) and is therefore about a factor of 300 lower for ^{15}N than for protons, which implies a factor of 100000 difference in measuring time. It has been demonstrated that the INEPT experiment (38,39) can alleviate this problem to a certain extent, but nevertheless detection remains difficult. Bodenhausen and Ruben (40) demonstrated that the ^{15}N frequency could be measured indirectly *via* the protons directly coupled to the ^{15}N nucleus. Their rather complicated sequence transfers proton magnetization to the ^{15}N, which then evolves during the evolution period of the 2D experiment, before being transferred back to the protons which are detected during the acquisition time in this experiment. A much simpler alternative, that relies on the same principle as this "Overbodenhausen experiment" has been proposed rather recently (41,42). Experimental results indicate that with this new experiment

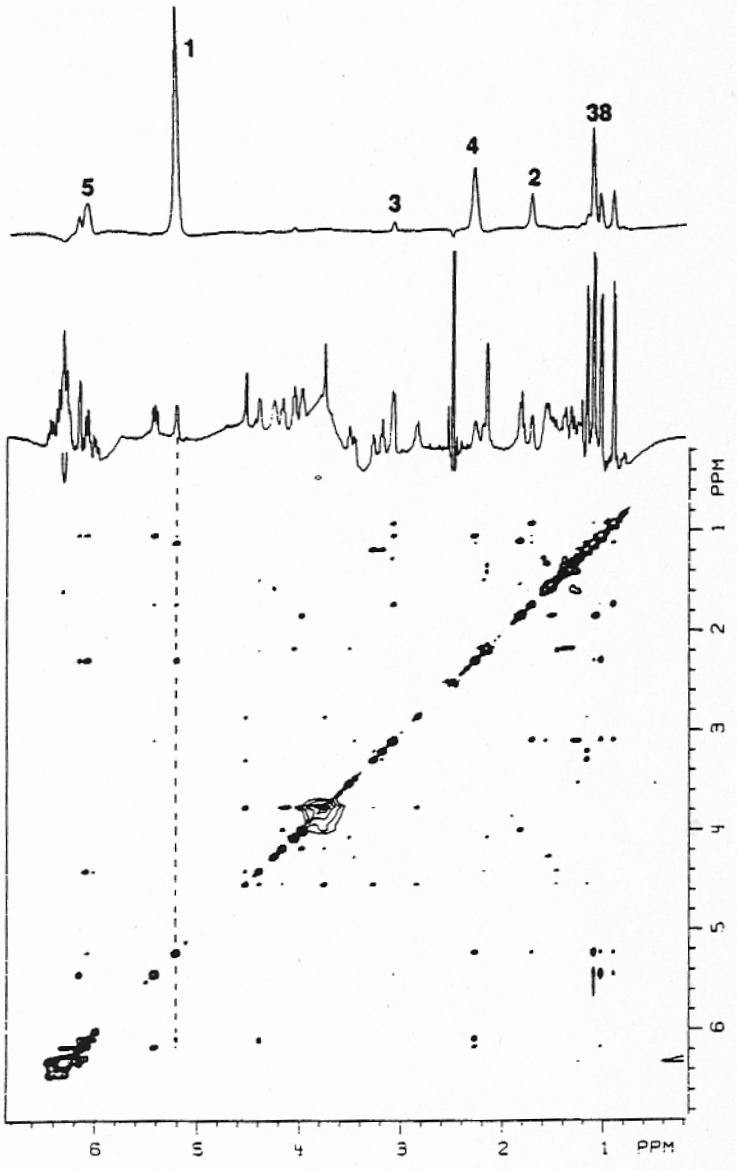

Figure 12. Two-dimensional NOE spectrum of amphotericin B, recorded at 500 MHz, using a mixing time of 200 ms. The top trace displays the cross-section taken through the 2D spectrum at the chemical shift of H1, showing spacial proximity to Me39, Me40, H2, H4, and H5. The cross-peak with H3 (3.12 ppm) is much lower in intensity suggesting a larger distance. The mixing time (200 ms) is not short enough to exclude relayed NOE effects, and quantitative interpretation of cross peak intensities is not feasible from this single spectrum.

the theoretical enhancement factor of 300 really can be obtained (43). The experiment works only for protonated ^{15}N nuclei. Consider the energy level diagram of an isolated ^{1}H-^{15}N pair (Figure 13). The broken lines represent the two (weak)

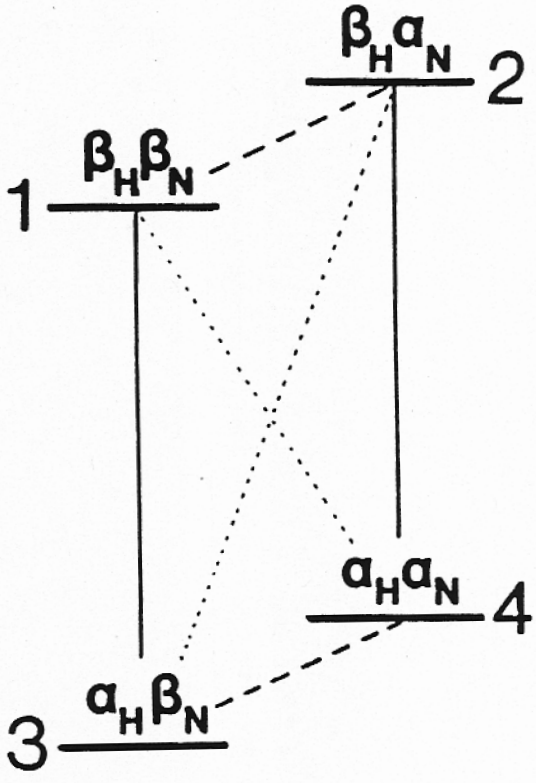

Figure 13. Energy level diagram and wave functions for a ^{15}N-^{1}H spin pair. The insensitive ^{15}N resonances (broken lines) are measured indirectly by measuring the zero and double quantum resonances (dotted lines) via the proton resonances (solid lines).

^{15}N transitions. The solid lines represent the (intense) proton transitions. The basic concept of the new experiment is to generate the dotted transitions (zero and double quantum), that resonate with frequencies $\Omega_H \pm \Omega_N$. If those frequencies are measured indirectly, with a 2D experiment, the ^{15}N frequency can be calculated since the proton frequency, Ω_H, is known.

The pulse scheme of the experiment is shown in Figure 14. The ^{1}H 180° pulse at the center of the evolution period and the ^{15}N decoupling during data acquisition are optional and will, at first, not be taken into account. The theory of the

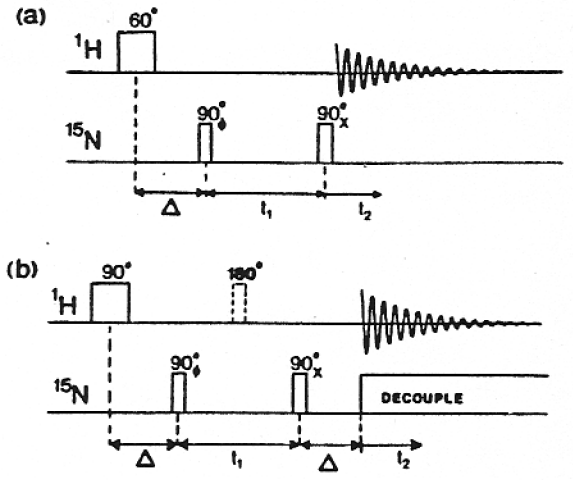

Figure 14. Pulse scheme of the experiment for indirect detection of ^{15}N through multiple quantum coherence. The first pulse applied to the protons can be of the Redfield type or of the 1-3-3-1 type and does not require additional phase cycling. (b) The 180° ^{1}H pulse applied at the center of the evolution period interchanges zero and double quantum coherence and causes elimination of the ^{1}H frequency contribution in the F_1 dimension, leading to a regular heteronuclear shift correlation spectrum. The ^{15}N decoupling during acquisition removes heteronuclear coupling from the F_2 dimension and, in principle, doubles the sensitivity of the experiment. In both (a) and (b), the phase of the first 90° ^{15}N pulse is cycled according to Table 3.

Table 3. Phase of the first ^{15}N pulse in the pulse scheme of Fig. 14 and the mode of data collection for detection of the double (DQ) and of the zero quantum (ZQ) component.

Step	ϕ	DQ	ZQ
1	x	x	x
2	y	-y	y
3	-x	-x	-x
4	-y	y	-y

experiment is most easily described with the operator formalism, treated in section ID. The proton 90° pulse creates magnetization along the -y axis of the rotating frame, which then evolves for a time Δ:

$$I_{Hy} \xrightarrow{(\Omega_H + 2\pi J_{NH} I_{Hz} I_{Nz})\Delta}$$

$$\{I_{Hy}\cos(\Omega_H\Delta) - I_{Hx}\sin(\Omega_H\Delta)\}\cos(\pi J_{NH}\Delta) + 2\{-I_{Hx}\cos(\Omega_H\Delta) - I_{Hy}\sin(\Omega_H\Delta)\}\sin(\pi J_{NH}\Delta)I_{Nz} \quad (24)$$

If the delay, Δ, is set to $1/(2J_{NH})$, only the second term at the right hand side of expression 24 survives, and a 90°$_x$ ^{15}N pulse applied at this time will generate product terms $I_{Hx}I_{Ny}$ and $I_{Hy}I_{Ny}$. The sine and cosine coefficients will be omitted to simplify the expressions. During the evolution period, those product terms evolve according to:

$$I_{Hx}I_{Ny} \xrightarrow{\Omega_H t_1 + \Omega_N t_1}$$

$$[\cos(\Omega_H t_1)I_{Hx} + \sin(\Omega_H t_1)I_{Hy}] \times$$

$$[\cos(\Omega_N t_1)I_{Ny} - \sin(\Omega_N t_1)I_{Nx}] \quad (25)$$

The final 90° ^{15}N pulse converts those two-spin coherences back into observable ^{1}H magnetization. If all terms are taken into account, a 90°$_x$ ^{15}N pulse generates an observable signal:

$$s(t_1, t_2) =$$

$$M_{oH}\exp[i(\Omega_H \pm \pi J_{NH})(t_1 + t_2)]\cos(\Omega_N t_1) \quad (26a)$$

and if the first 90° ^{15}N pulse were applied along the -y axis, the second 90° ^{15}N pulse generates

$$s(t_1, t_2) =$$

$$M_{oH}\exp[i(\Omega_H \pm \pi J_{NH})(t_1 + t_2)]\sin(\Omega_N t_1) \quad (26b)$$

If either of those two signals is used separately to calculate a 2D spectrum, two resonances in ing the zero and double quantum frequencies, respectively. The results of eqns. 26a and 26b can be combined in the usual fashion (eqns. 6 and 11) to give either the double or the zero quantum frequency in the 2D spectrum. Because the zero quantum resonance in the 2D spectrum

is centered at $(\omega_1,\omega_2) = (\Omega_N+\Omega_H,\Omega_H)$, the computer can subtract a frequency ω_2 from all ω_1 coordinates, to yield a pure chemical shift correlation map, with resonances centered at (Ω_N,Ω_H). Broad-band ^{15}N decoupling during the detection period can be used to eliminate the effect of heteronuclear coupling in this experiment.

If the first ^{15}N 90° pulse is applied along the -x axis, the signal of eqn. 26a will be detected with opposite sign. Since signals from protons not coupled to ^{15}N will not know about this phase shift and their shape will be unchanged in the two experiments, subtraction of the two experiments will give cancellation of the signals of protons that are not coupled to ^{15}N. Hence, the ^{15}N satellites in the ^{1}H spectrum can therefore be detected, not hampered by the 600 times stronger signal from protons coupled to ^{14}N. In total four experiments will be performed for every t_1 value, with the phase of the first ^{15}N pulse cycled along all four axes.

As an example, Figure 15 shows the zero and double quantum spectra of a 30 mM solution of α-thymosin, dissolved in 90% H_2O/10% D_2O. Spectra were recorded on a modified Nicolet 300 MHz instrument, and the total measuring time was approximately 12 h. The signals of eqns. 26a and 26b were stored in separate locations and spectrum (a) was computated from the double quantum signals and (b) was computated from the zero quantum signals, using the same two sets of acquired data.

In practice, application of the sequence of Figure 14b can sometimes be more difficult for natural abundance samples than the sequence of Figure 14a. This is due to the high power ^{15}N decoupling during data acquisition, which can cause a slight perturbation of the ^{2}H lock signal. A very stable lock signal is required to allow complete elimination of the 600 times stronger signal from protons coupled to ^{14}N.

As pointed out in Section I, it is desirable to record spectra in the absorption mode, both from a viewpoint of sensitivity as well as resolution. However, in this experiment the data are truely phase modulated (not artificially induced). Conversion to amplitude modulation is possible by insertion of a 180° pulse at the center of the evolution period (44). However, in the case where the proton also has homonuclear coupling, phase modulation cannot be avoided and pure absorption mode spectra cannot be recorded. A nice feature of the simplest form of the experiment is that it utilizes only one pulse for the observed protons. This pulse can be of arbitrary flip angle; a small flip angle allows a faster repetition rate and consequently will yield somewhat higher sensitivity. More important is the fact that any type of pulse can be used for this proton excitation. For example, a Redfield water suppression or a 1-3-3-1 water suppression pulse

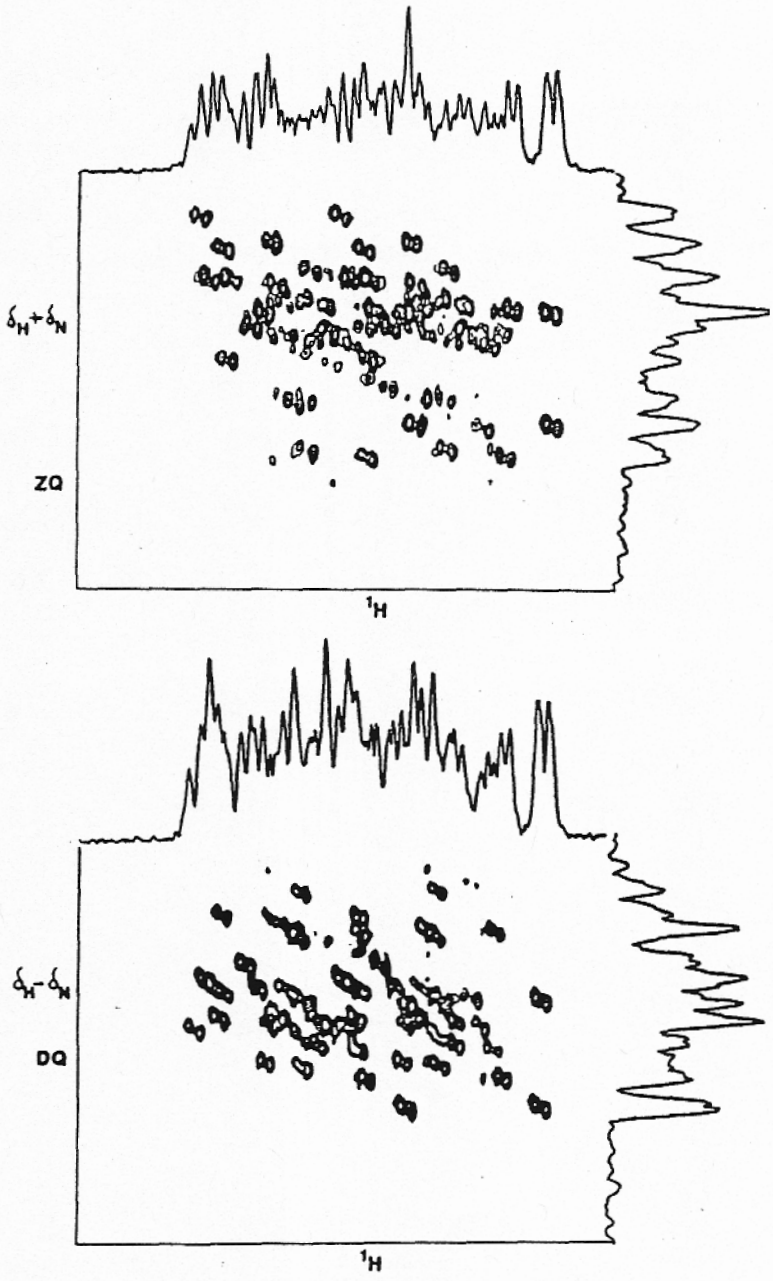

Figure 15. Zero and double quantum natural abundance ^{1}H-^{15}N spectra of a 30 mM solution of α-thymosin in H_2O. Spectra were recorded on a modified Nicolet 300 MHz instrument, and both spectra are obtained from the same set of acquired data. The total measuring time was approximately 12 h. The spectra were kindly provided by Dr. David Live and Dr. Donald Davis.

can be used, making it feasible to use this experiment in H_2O solution. Of course, the experiment is not limited to the indirect detection of ^{15}N resonances. The technique has also great promise for metabolic NMR studies in vivo, by using ^{13}C labeled starting material.

V. DISCUSSION

Although only a small number out of the large collection of two-dimensional NMR experiments has been treated here, it will be clear that the 2D approach extends the capabilities of NMR experiments enormously. Many applications of 2D NMR in organic and biochemistry have appeared in the recent literature. On modern NMR spectrometers, utilization of the various two-dimensional experiments has become rather simple by the introduction of suitable support software and spectrometer documentation. The main problem the inexperienced spectroscopist has to face is which experiment to choose and which results to expect. A comprehensive guide on this subject has not yet appeared, but in general it is usually a good idea to apply the standard experiments before attempting to use a more sophisticated version of those experiments. It is expected that the number of experimental pulse schemes still will expand significantly, but once the spectroscopist realizes that all those methods are small variations on the same theme, the collection of 2D experiments will appear less bewildering and practical application of those techniques becomes much simpler.

ACKNOWLEDGMENT

I wish to thank Ingrid Pufahl for typing and editing most of the manuscript. I am also indebted to Dr. David Live and to Dr. Donald Davis for providing the spectra of Figure 15 and to Dr. A. Aszalos for providing the sample of Amphotericin B and for interpretation of the corresponding spectra that resulted in complete assignment of the ^1H spectrum.

REFERENCES

[1] J. Jeener, *Ampere International Summer School*, Basko polje, Yugoslavia (1971).

[2] G. Bodenhausen, R. Freeman, R. Niedermeyer and D.L. Turner, *J. Magn. Reson.* **26** 133 (1977).

[3] W. P. Aue, P. Bachmann, A. Wokaun and R. R. Ernst, *J. Magn. Reson.* **29,** 523 (1978).

[4] A. Bax and T. H. Mareci, *J. Magn. Reson.* **53,** 360 (1983).

[5] M. H. Levitt, G. Bodenhausen, and R. R. Ernst, *J. Magn. Reson.* **58,** 462 (1984).

[6] D. L. Turner, *J. Magn. Reson.* **58,** 500 (1984).

[7] P. Bachmann, W. P. Aue, L. Mueller and R. R. Ernst, *J. Magn. Reson.* **28,** 29 (1977).

[8] A. Bax, A. F. Mehlkopf and J. Smidt, *J. Magn. Reson.* **40,** 213 (1980).

[9] A. deMarco and K. Wuethrich, *J. Magn. Reson.* **24,** 201 (1976).

[10] A. Bax, G. A. Morris and R. Freeman, *J. Magn. Reson.* **43,** 333 (1981).

[11] I. D. Campbell, C. M. Dobson, R. J. P. Williams, and A. V. Xavier, *J. Magn. Reson.* **11,** 172 (1973).

[12] L. Mueller and R. R. Ernst, *Mol. Phys.* **38,** 963 (1979).

[13] R. Freeman, S. P. Kempsell and M. H. Levitt, *J. Magn. Reson.* **34,** 663 (1979).

[14] D. J. States, R. A. Haberkorn and D. J. Ruben, *J. Magn. Reson.* **48,** 286 (1982).

[15] G. Bodenhausen, H. Kogler and R. R. Ernst, *J. Magn. Reson.* **58,** 370 (1984).

[16] G. Drobny, A. Pines, S. Sinton, D. Weitekamp and D. Wemmer, *Faraday Div. Chem. Soc. Symp.* **13,** 49 (1979).

[17] A. G. Redfield and S. D. Kunz, *J. Magn. Reson.* **19,** 250 (1975).

[18] See, for example, T. C. Farrar and E. D. Becker, *Pulse and Fourier Transform NMR*, Academic Press, New York (1971).

[19] O. W. Sorensen, G. W. Eich, M. H. Levitt, G. Bodenhausen and R. R. Ernst, *Progr. in NMR Spectroscopy* **16,** 163 (1983).

[20] K. J. Packer and K. M. Wright, *Mol. Phys.* **50,** 797 (1983).

[21] F. J. M. van de Ven and C. W. Hilbers, *J. Magn. Reson.* **54,** 512 (1983).

[22] W. P. Aue, E. Bartholdi and R. R. Ernst, *J. Chem. Phys.* **64,** 2229 (1976).

[23] A. Bax and R. Freeman, *J. Magn. Reson.* **44,** 542 (1981).

[24] K. Nagayama, A. Kumar, K. Wuethrich and R. R. Ernst, *J. Magn. Reson.* **40,** 321 (1980).

[25] A. Bax, R. Freeman and G. A. Morris, *J. Magn. Reson.* **42,** 164 (1982).

[26] G. Wider, S. Macura, A. Kumar, R. R. Ernst and K. Wuethrich, *J. Magn. Reson.* **56,** 207 (1984).

[27] D. Marion and K. Wuethrich, *Biochem. Biophys. Res. Commun.* **113,** 967 (1983).

[28] A. Bax, *Two-Dimensional NMR in Liquids*, Reidel, Boston, 1982, Chpt. 2.

[29] D. I. Hoult and R. E. Richards, *Proc. Roy. Soc. London, Ser. A.* **344,** 311 (1975).

[30] U. Piantini, O. W. Sorensen and R. R.

Ernst, *J. Am. Chem. Soc.* **104,** 6800 (1982).

[31] A. Bax, R. A. Byrd and A. Aszalos, *J. Am. Chem. Soc.*, **106,** 7632 (1984).

[32] J. Jeener, B. H. Meier, P. Bachmann and R. R. Ernst, *J. Chem. Phys.* **71,** 4546 (1979).

[33] S. Macura and R. R. Ernst, *Mol. Phys.* **41,** 95 (1980).

[34] W. Braun, G. Wider, K. H. Lee and K. Wuethrich, *J. Mol. Biol.* **169,** 921 (1983).

[35] W. Braun, C. Boesch, L. R. Brown, N. Go and K. Wuethrich, *Biochem. Biophys. Acta* **667,** 377 (1981).

[36] S. Macura, K. Wuethrich and R. R. Ernst, *J. Magn. Reson.* **46,** 269 (1982).

[37] A. Minoretti, W. P. Aue, M. Reinhold and R. R. Ernst, *J. Magn. Reson.* **40,** 175 (1980).

[38] G. A. Morris and R. Freeman, *J. Am. Chem. Soc.* **101,** 760 (1979).

[39] D. P. Burum and R. R. Ernst, *J. Magn. Reson.* **39,** 163 (1980).

[40] G. Bodenhausen and D. J. Ruben, *Chem. Phys. Lett.* **69,** 185 (1980).

[41] A. Bax, R. H. Griffey and B. L. Hawkins, *J. Am. Chem. Soc.* **105,** 7188 (1983).

[42] A. Bax, R. H. Griffey and B. L. Hawkins, *J. Magn. Reson.* **55,** 301 (1983).

[43] D. H. Live, D. G. Davis, W. C. Agosta and D. Cowburn, *J. Am. Chem. Soc.* **1056,** 6104 (1984).

[44] L. Mueller, *J. Am. Chem. Soc.* **101,** 4481 (1979).